ISSN 0036-0236, Russian Journal of Inorganic Chemistry, 2023, Vol. 68, No. 4, pp. 379–385. © Pleiades Publishing, Ltd., 2023.
ISSN 0036-0236, Russian Journal of Inorganic Chemistry, 2023. © Pleiades Publishing, Ltd., 2023.
Russian Text © The Author(s), 2023, published in Zhurnal Neorganicheskoi Khimii, 2023, Vol. 68, No. 4, pp. 444–451.

SYNTHESIS AND PROPERTIES OF INORGANIC COMPOUNDS

Thermal Stability of Nanocrystalline Zinc Sulfide ZnS

S. I. Sadovnikov[a], * and S. V. Sergeeva[b]

[a] *Institute of Solid-State Chemistry, Ural Branch, Russian Academy of Sciences, Yekaterinburg, 620990 Russia*
[b] *Institute of Metallurgy, Ural Branch, Russian Academy of Sciences, Yekaterinburg, 620016 Russia*
**e-mail: sadovnikov@ihim.uran.ru*

Received November 8, 2022; revised January 10, 2023; accepted January 11, 2023

Abstract—Nanocrystalline zinc sulfide (ZnS) powders are prepared via hydrothermal deposition from aqueous solutions of zinc nitrate and sodium sulfide in the presence of sodium citrate or Trilon B. The average particle sizes of the product ZnS nanopowders ranging from 2 to 9 nm are tuned via varying the batch concentrations of the reagents. Air-annealing of as-prepared ZnS nanopowders at temperatures of 280 to 530°C oxidizes cubic zinc sulfide to hexagonal zinc oxide. The oxidation of the finest-grained zinc sulfide nanopowders having a particle size of 2 nm starts at 280–330°C, while the coarsest-grained nanopowder having a particle size of 9 nm starts to oxidize at 530°C. In the coarsest-grained ZnS powder, the particle size increases as little as from 9 to 12 nm when temperature rises to 530°C, while the finest-grained nanopowders have their particle sizes increase from 2 to 9 nm in response to the same rise in temperature.

Keywords: chemical deposition, phase and size stability, zinc oxide
DOI: 10.1134/S0036023623600120

INTRODUCTION

The low-temperature cubic (space group $F\bar{4}3m$) polymorph α-ZnS has the sphalerite cubic structure (*B*3 type) and is stable at temperatures below 1290 K. At 1293 K, the low-temperature cubic zinc sulfide phase transforms to the high-temperature hexagonal (space group $P6_3mc$) polymorph β-ZnS with the wurtzite structure. Bulk zinc sulfide under normally is a wide-gap semiconductor. The bandgap E_g of cubic α-ZnS is ca. 3.50–3.76 eV, the E_g of hexagonal wurtzite β-ZnS is ca. 3.74–3.91 eV [1–3]. The exciton diameter of bulk zinc sulfide is 4.8–5.2 nm [3]. Polytype structures typical of hexagonal wurtzite can appear in nanosized zinc sulfide particles.

Zinc sulfide ZnS is one of the most used semiconductor sulfides [4, 5] along with lead, silver, copper, and cadmium sulfides. Zinc sulfide is used in ultrasound amplifiers and detectors, infrared sensors, near- and mid-IR lasers. Especially often zinc sulfide is used as a phosphor in luminescent devices, solar cells, LEDs, and liquid crystal displays [3–8]. The electronic properties of nanocrystalline zinc sulfide, as the properties of other sulfide semiconductors, too, differ significantly from the properties of the respective bulk material [3]. Zinc sulfide nanoparticles with <10 nm sizes are manufactured in liquid media, specifically in microemulsions [9], in aqueous colloidal solutions of zinc nitrate or zinc sulfate and sodium sulfide using 3-mercaptopropyltrimethoxysilane as a stabilizer [10], or in aqueous solutions of zinc nitrate and sodium sulfide [11] with Trilon B (ethylenediaminetetraacetic acid) as a stabilizer.

The thermal stability of the size of ZnS nanoparticles and their phase assemblage is a critical parameter for the usefulness of nanocrystalline ZnS. Nanocrystalline zinc sulfide can oxidize under heating. Therefore, in order to expand the application of nanocrystalline zinc sulfide, one needs to know how stable the size and phase composition of ZnS nanoparticles are. The relevant information on nanocrystalline zinc sulfide is scarce. Shanmugam et al. in their study of the behavior of ZnS nanoparticles [12] found out that zinc sulfide nanoparticles fully oxidize to zinc oxide at 500°C. Mohamed and Abdel-Kader considered the effect of temperature on the stability of optical properties of PVA/ZnS nanocomposites [13]; annealing temperatures higher than 300°C caused the decay of optical properties of the nanocomposites. Queiroz et al. [14] considered the behavior of bulk ZnS and found out that oxidation started at rather high temperatures (>610°C). Osuntokun and Ajibade [15, 16] showed that the thermal stability of a nanocomposite comprising ZnS nanoparticles embedded in a polyvinyl alcohol (PVA) polymer matrix was higher than the thermal stability of individual PVA.

Here, we were the first to study the effect of temperature on the compositional stability of zinc sulfide nanoparticles and to determine the effect of the nanoparticle size on the oxidation onset temperature. The thermal stability of the particle size was studied in zinc sulfide nanoparticles having as-prepared sizes

Table 1. Batch compositions, unit cell parameter a and average particle size D in the prepared ZnS nanopowders

No.	Batch concentrations of the reagents, mmol/L				a_{B3}, nm	$D \pm 0.5$, nm (XRD)
	$Zn(NO_3)_2$	Na_2S	Na_3Cit	EDTA-H_2Na_2		
1*	50	50	–	–	0.5357	2
2**	100	100	–	–	0.5332	2.5
3*	50	50	6.25	–	0.5333	3.5
4***	50	100	–	5	0.5395	9

* The exposure time of ZnS nanoparticles prepared in batches **1** and **3** was 2–3 min. ** The exposure time of ZnS nanoparticles prepared in batch in batch **2** was 20 h. ***The exposure time of ZnS nanoparticles prepared in batch **4** was 70 h.

from 2 to 9 nm, manufactured with various concentrations of precursors. The choice of sodium citrate as the stabilizer was dictated by the fact that it is the most popular and chemically unhazardous antioxidant and would provide the formation of a single sulfide phase, in our case, ZnS. As to Trilon B, this is a universal complex former to provide small-sized nanoparticles.

EXPERIMENTAL

Nanocrystalline zinc sulfide powders were manufactured by chemical deposition from aqueous solutions of zinc nitrate $Zn(NO_3)_2$ and sodium sulfide Na_2S. Aqueous solutions of sodium citrate ($Na_3C_6H_5O_7 \equiv Na_3Cit$) and disodium salt of ethylenediaminetetraacetic acid (EDTA-H_2Na_2 ≡ Trilon B) served as complex-forming agents and stabilizers. The details of the synthetic procedure to prepare ZnS nanopowders are described elsewhere [11].

The batch compositions were as shown in Table 1. The batch concentration of $Zn(NO_3)_2$ was 50 or 100 mmol/L. Aqueous solutions were sonicated for 30 min using a Bandelin SONOPULS HD 2070 ultrasonic homogenizer for providing a uniform distribution of the synthesized nanoparticles. The synthesis temperature was 298–323 K. The exposure time of nanoparticles in the batch was 2–3 min for samples **1** and **2**, 20 h for sample **3**, and 70 h for sample **4**.

The prepared powders were washed by decantation and then freeze-dried in an Alpha 1-2 LDplus (Martin Christ) freeze-dryer at an ice condenser temperature of –55°C (218 K). The dried nanocrystalline zinc sulfide powders were stored in a Sanplatec MB Vacuum Desiccator under a residual pressured of 13.3 Pa (0.1 mmHg).

The microstructure, size, and elemental chemical composition of ZnS nanoparticles in colloidal solutions were determined by transmission electron microscopy (TEM) on a Jeol JEM-2010 electron microscope with a grating resolution of 140 pm (1.4 Å). The elemental chemical composition of ZnS nanoparticles was studied using the same microscope supplemented with a Phoenix (EDAX) energy-dispersive spectrometer (a Si(Li) detector with the 130-eV energy resolution). For use in experiments, colloidal solutions of ZnS nanoparticles were spread over a copper grid pre-coated with one or two layers of collodion glue (a colloxylin solution in ethanol). After the adhesive coating dried, a carbon-containing mesh with voids remained. The details of the TEM experiments are described elsewhere [17].

The thermal stability of zinc sulfide was determined as follows: a sample of weight m was placed in a muffle furnace preheated to the required temperature and exposed to this temperature under air for 2 h; then, the annealing-induced weight change Δm was determined.

The as-deposited sulfide powders and the same powders after air-annealing at various temperatures were studied by X-ray diffraction on a Shimadzu XRD-7000 diffractometer (the details of the measurement procedure are described elsewhere [18]). The final structure refinement for the synthesized sulfide powders was carried out using the X'Pert Plus software package [19]. The qualitative and quantitative phase composition of the precipitated powders was estimated using the Match Version 1.10b software package [20].

RESULTS AND DISCUSSION

High-resolution transmission electron microscopy (HRTEM) served to estimate the particle sizes of the ZnS nanoparticles prepared in batches **1**–**4**. Figure 1 shows the HRTEM images of agglomerated ZnS nanoparticles prepared in batches **1** and **3**, which have average particles sizes of ca. 2 to ca. 4 nm, respectively. The highlighted areas in the HRTEM images correspond to cubic (space group $F\bar{4}3m$) zinc sulfide with the sphalerite (α-ZnS) structure.

The zinc and sulfur concentrations as probed by energy-dispersive X-ray analysis in the zinc sulfide powders washed by distilled water and vacuum-dried are 67.0 ± 0.3 wt % Zn and 32.8 ± 0.3 wt % S in the powders with average particle sizes of ca. 2 nm, and 67.1 ± 0.3 wt % Zn and 32.7 ± 0.2 wt % S in those having average particle sizes of ca. 9 nm; these concentrations correspond to stoichiometric ZnS.

Figure 2 shows representative X-ray diffraction patterns of the zinc sulfide powders deposited from batches **1**–**4** (Table 1). All nanopowders give signifi-

cantly broadened diffraction reflections due to the small ZnS particle sizes. The particle size D of ZnS nanopowders derived from the diffraction reflection broadening is 2 to 9 nm (Table 1). Our quantitative analysis and comparison with the literature data [21, 22] showed that the observed set of diffraction reflections correspond to single-phase zinc sulfide with the sphalerite-type cubic (space group $F\bar{4}3m$) structure. The lattice period a_{B3} of the synthesized ZnS nanopowders is ca. 0.5332–0.5395 nm.

The annealing temperature, which changes the composition and structure of products, accordingly affects the X-ray diffraction patterns of zinc sulfide nanopowders. To illustrate this, Figs. 3 and 4 show the X-ray diffraction patterns for zinc sulfide nanopowders **1** and **4** with the finest and coarsest nanoparticles, respectively.

Figure 3 shows the evolution of the X-ray diffraction patterns of zinc sulfide nanopowder **1** with an as-synthesized particle size of ca. 2 nm induced by air annealing at temperatures in the range from 180 to 530°C. The particle size remains almost unchanged after annealing at temperatures up to 180°C. When the annealing temperature rises to 230 and 330°C, the zinc sulfide particles grow in size to 3 and 5 nm, respectively. Our quantitative analysis and comparison to the related literature [21–23] showed that the oxidation of zinc sulfide nanopowders to yield hexagonal (space group $P6_3mc$) ZnO during annealing starts at 280°C, when weak $(002)_{ZnO}$ and $(101)_{ZnO}$ reflections appear in the X-ray diffraction pattern (Fig. 3). At annealing temperature above 280°C, the number of zinc oxide diffraction reflections becomes progressively greater and they grow in intensity. When the annealing temperature is 480°C, the amount of the oxide phase (ZnO) and the particle sizes of the oxide and sulfate phases become slightly greater. After annealing at 530°C, the amount of the oxide phase reaches 21 wt % and the ZnS and ZnO particle sizes become ca. 10 and ca. 20 nm, respectively. At 530°C, the oxide phase amounts to 30 wt % and the ZnS and ZnO particle sizes are ca. 20 and ca. 30 nm, respectively. It is pertinent to mention here that in the X-ray diffraction patterns of nanopowder **1** recorded after it was annealed at 480 and 530°C, there is a line to the left of the $(111)_{ZnS}$ line around $2\theta = 27.1°$ that can be indexed as the $(100)_{ZnS2H}$ reflection from hexagonal wurtzite ZnS of the 2H polytype [24], although wurtzite can exist at temperatures above 1020°C. This can be due to the formation of a polytype structure in nanosized zinc sulfide.

Figure 4 illustrates the evolution of the X-ray diffraction patterns of zinc sulfide nanopowder **4**, whose as-prepared particle size was ca. 9 nm, induced by annealing in air at temperatures up to 530°C. The nanoparticle size remains almost unchanged until the sample is annealed at 380°C. Annealing at 430°C increases the particle size to ca. 10 nm. The oxidation

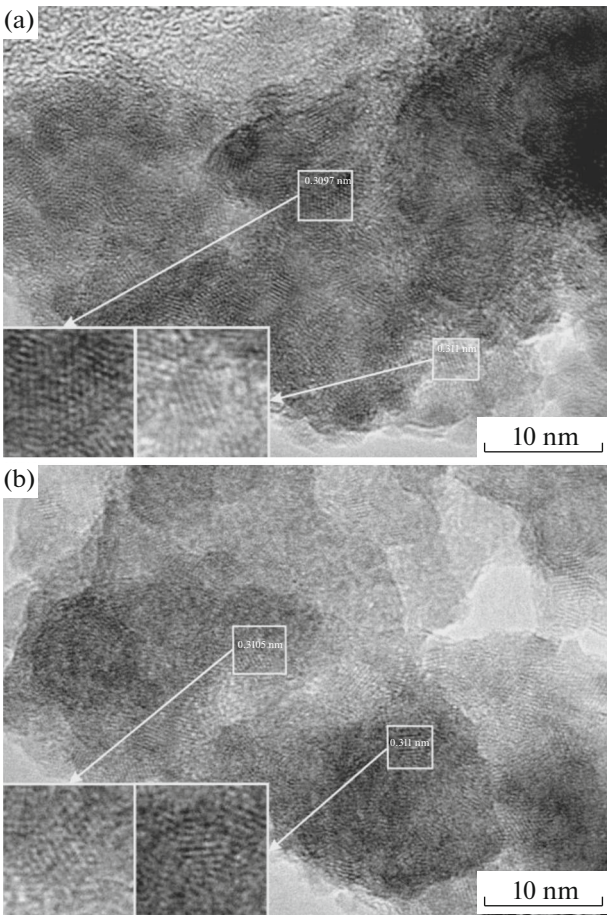

Fig. 1. HRTEM images of agglomerated nanocrystalline ZnS particles produced from (a) batch **1** and (b) batch **3**. The highlighted areas refer to cubic (space group $F\bar{4}3m$) zinc sulfide with the sphalerite α-ZnS structure. The observed interplanar distances (ca. 0.310–0.311 nm) coincide with the distances between the (111) atomic planes of cubic (space group $F\bar{4}3m$) zinc sulfide α-ZnS. The bottom left insets in panels (a) and (b) show magnified highlighted areas.

of nanopowder **4** to form zinc oxide starts only at 530°C. At this annealing temperature, the ZnS particle size increases to ca. 12 nm, and the ZnO particle size at 530°C is ca. 27 nm. The ZnO percentage in nanopowder **4** at 530°C is 13 wt %.

The X-ray diffraction patterns of zinc sulfide nanopowders **2** and **3** with an as-prepared particle size of ca. 2.5 and ca. 3.5 nm, annealed in air at temperatures up to 480 and 530°C, respectively, are intermediate between the X-ray diffraction patterns of nanopowders **1** and **4**. A specific feature of nanopowder **2** is its nearly constant particle size until it is annealed at 430°C, while in nanopowder **3**, the particle size starts increasing at 280°C. The oxidation of nanopowders **2** and **3** to yield ZnO starts at 330–380°C. The ZnS particle size in nanopowder **3** at 530°C is ca. 12 nm, and the ZnO particle size is ca. 25 nm. The ZnO percentage in nanopowder **3** at 530°C is 22 wt %.

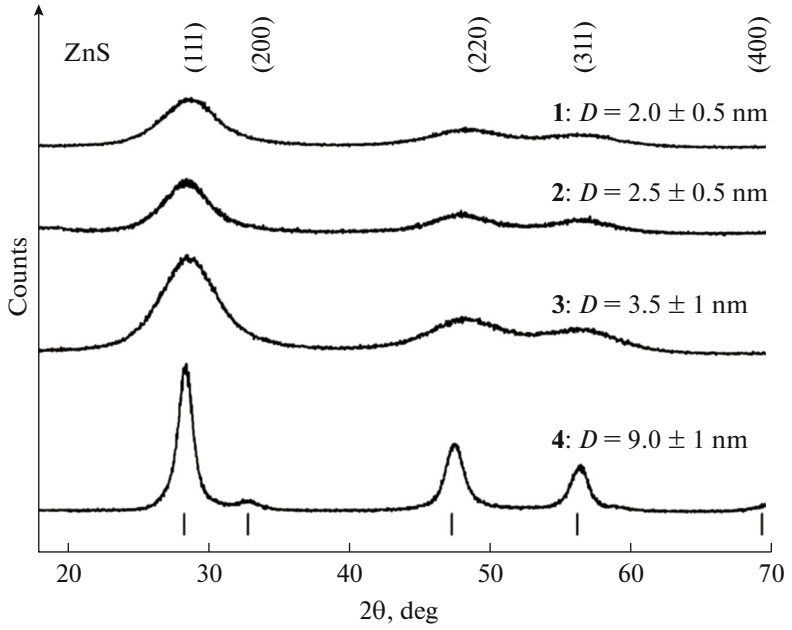

Fig. 2. X-ray diffraction patterns of nanosized ZnS, powders deposited from batches **1**–**4**.

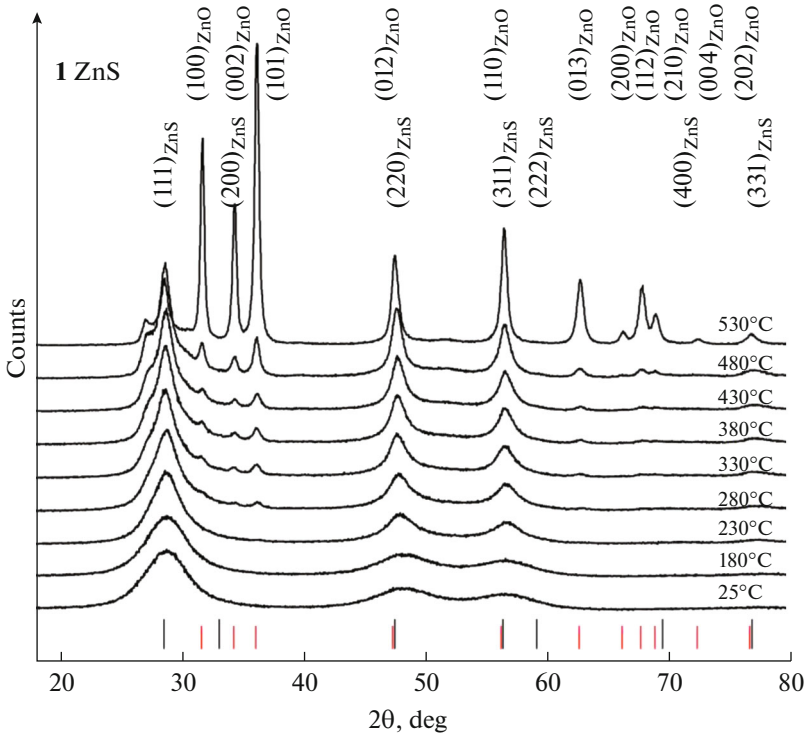

Fig. 3. Evolution of the X-ray diffraction pattern of nanocrystalline zinc sulfide powder **1** having an as-prepared particle size of ca. 2 nm upon a rise in annealing temperature from 180 to 530°C. The long black and short red strikes indicate the reflection position for cubic (space group $F\bar{4}3m$) zinc sulfide ZnS and hexagonal (space group $P6_3mc$) zinc oxide, respectively.

The above results show that the finest-grained zinc sulfide nanopowders **1** and **2** start to oxidize at lower temperatures when annealed in air (the diffraction reflections from zinc oxide ZnO in sample **1**, where the particle size is ca. 2 nm, appear when the annealing temperature is 280°C, while in sample **3**, where the particle size is ca. 3.5 nm, oxidation starts when the annealing temperature is 330°C). Thus, the onset oxi-

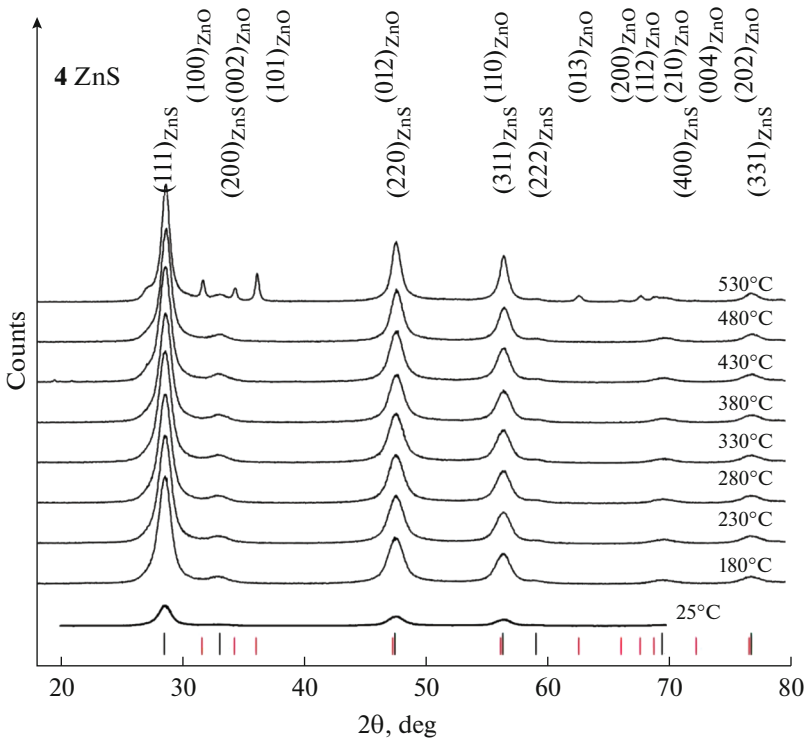

Fig. 4. Evolution of the X-ray diffraction pattern of nanocrystalline zinc sulfide powder **4** having an as-prepared particle size of ca. 9 nm upon a rise in annealing temperature from 180 to 530°C. The long black and short red strikes indicate the reflection position for cubic (space group $F\bar{4}3m$) zinc sulfide ZnS and hexagonal (space group $P6_3mc$) zinc oxide, respectively.

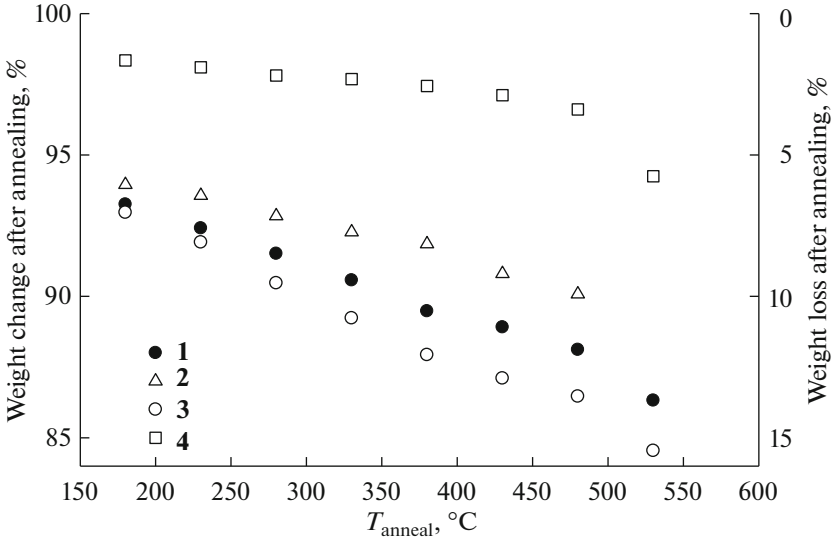

Fig. 5. Weight change of ZnS powders after air-annealing at 180–530°C. The nanopowders are numbered to match their numbering in Table 1.

dation temperature of the finest-grained zinc sulfide nanopowders is 280–330°C, against as high a temperature as 530°C for the coarsest-grained nanopowder. The particle size of the coarsest-grained ZnS powder increases as little as from 9 to 12 nm (by ca. 30%) when the temperature rises to 530°C, while in the finest-grained nanopowders, the same temperature elevation brings about an increase in particle size from 2 to 9 nm, i.e., nearly by five times.

The subject matter of this work is the thermal stability of ZnS nanoparticles. The effect of the batch ratio of the precursors on the ZnS nanoparticle size was studied previously [11]; also see works on the thermal stability and oxidation of lead sulfide [25, 26].

In all cases, annealing of ZnS powder samples leads to weight loss Δm, which increases as the annealing temperature rises (Fig. 5). Part of the weight loss is due to the oxidation of some ZnS to ZnO, whose formula weight is smaller than the ZnS formula weight. The ZnO percentage in samples **1**, **3**, and **4** after annealing at 530°C, as determined by X-ray powder diffraction, is 30, 22, and 13 wt %, respectively, in match with the oxidation-induced weight loss of ca. 5.0, ca. 3.6, and ca. 2.1 wt %, respectively. Apparently, the rest of the observed weight loss is mainly due to the evaporation of the air moisture adsorbed by nanopowders.

Indeed, nanopowders are very hygroscopic, and their water uptake is the greater, the smaller is their particle size [27, 28]. The water vapor uptake by GaN, PbS, and CdS nanopowders from the air increases as their particle sizes decrease and the relative air humidity rises [29–31].

In view of the weight losses of nanopowders measured upon ZnS oxidation to ZnO and the literature data on the water uptake and hygroscopicity of sulfide and nitride powders [29–31], we may suggest that the weight loss from zinc sulfide powders **1**–**4** is due to removal their adsorbate water, which ranges between about 9–10 and about 3–4%. The weight changes imply that the finest nanopowders **1**–**3** with particle sizes of 2.0–3.5 nm contain greater amounts of adsorbate water, while the coarsest-grained nanopowder **4** with a particle size of ca. 9 nm has the least water uptake from the air. Some weight loss from ZnS nanopowders is also due to partial oxidation of sulfur and its elimination in the form of gaseous SO_2, as observed in the oxidation of silver sulfide nanopowders [32].

CONCLUSIONS

Nanocrystalline powders of cubic zinc sulfide ZnS with the average particle sizes ranging from 2 to 9 nm have been prepared via hydrochemical deposition from aqueous solutions of zinc nitrate and sodium sulfide in the presence of sodium citrate or Trilon B. The finest-grained ZnS nanopowders having particle sizes of 2–3 nm have been prepared from zinc nitrate and sodium sulfide solutions free of complex formers and stabilizers with the shortest deposition times (2–3 min). We have been the first to study the thermal stability of the phase composition and particle size in zinc sulfide nanopowders. The air-annealing of ZnS nanopowders at temperatures ranging from 280 to 530°C changes their phase composition due to the oxidation of cubic zinc sulfide to hexagonal zinc oxide. The finest-grained zinc sulfide nanopowders start to oxidize at 280–330°C, and the zinc oxide percentage in these nanopowders annealed at 530°C amounts to ca. 30 wt %. The coarsest-grained ZnS nanopowder with an as-prepared particle size of 9 nm starts to oxidize at as high the temperature as 530°C. When the ZnS particle sizes decrease to the nanometer scale, their oxidation onset temperature lowers by ca. 250–300°C compared to that in bulk zinc sulfide powders, whose oxidation onset temperature is ca. 610°C [14, 33]. Unlike bulk ZnS powders, which hold their particle sizes almost unchanged when heated under air to 600–700°C, ZnS nanoparticles have their sizes increasing upon heating to the same temperature to an extent that is the greater, the smaller is the size of as-prepared nanoparticles. The different thermal behaviors of nanosized and bulk ZnS powders in air are largely due to the highly developed surfaces of nanopowders.

ACKNOWLEDGMENTS

The authors are grateful to E.Yu. Gerasimov for his assistance in the TEM studies.

FUNDING

This work was supported by Ministry of Science and Higher Education of the Russian Federation (project No. 19-79-10101-П, https://rscf.ru/project/19-79-10101/) at the Institute of Solid-State Chemistry, the Ural Branch of the Russian Academy of Sciences.

CONFLICT OF INTEREST

The authors declare that they have no conflicts of interest.

REFERENCES

1. N. Kaur, S. Kaur, J. Singh, et al., J. Bioelectron. Nanotechnol. **1**, 5 (2016). https://doi.org/10.13188/2475-224X.1000006
2. M. Cardona and G. Harbeke, Phys. Rev. **137**, A1467 (1965). https://doi.org/10.1103/PhysReV.137.A1467
3. S. I. Sadovnikov, A. A. Rempel, and A. I. Gusev, Russ. Chem. Rev. **87**, 303 (2018). https://doi.org/10.1070/RCR4803
4. X. Fang, T. Zhai, U. K. Gautam, et al., Prog. Mater. Sci. **56**, 175 (2011). https://doi.org/10.1016/j.pmatsci.2010.10.001
5. X. Wang, H. Huang, B. Liang, et al., Crit. Rev. Solid State Mater. Sci. **38**, 57 (2013). https://doi.org/10.1080/10408436.2012.736887
6. T. Kryshtab, V. S. Khomchenko, J. A. Andraca-Adame, et al., J. Lumin. **129**, 1677 (2009). https://doi.org/j.jlumin.2009.04.069
7. X. Ma, J. Song, and Z. Yu, Thin Solid Films **519**, 5043 (2011). https://doi.org/10.1016/j.tsf.2011.01.125
8. S. Ummartyotin and Y. Infahsaeng, Renewable Sustainable Energy Rev. **55**, 17 (2016). https://doi.org/10.1016/j.rser.2015.10.120
9. M. Yu. Koroleva, E. V. Gulyaeva, and E. V. Yurtov, Russ. J. Inorg. Chem. **57**, 320 (2012). https://doi.org/10.1134/S0036023612030151

10. Yu. V. Kuznetsova, I. D. Popov, and A. A. Rempel, AIP Conf. Proc. **2313**, 030021 (2020). https://doi.org/10.1063/5.0032224
11. S. I. Sadovnikov, A. V. Ishchenko, and I. A. Weinstein, J. Alloys Compd. **851**, 154846 (2020). https://doi.org/10.1016/j.jallcom.2020.154846
12. N. Shanmugam, C. Shanmugam, N. Kannadasan, et al., J. Nanomater. **351798** (2013). https://doi.org/10.1155/2013/351798
13. M. B. Mohamed and M. H. Abdel-Kader, Mater. Chem. Phys. **241**, 122285 (2020). https://doi.org/10.1016/j.matchemphys.2019.122285
14. C. A. R. Queiroz, R. J. Carvalho, and F. J. Moura, Brazil. J. Chem. Eng. **22**, 127 (2005). https://doi.org/10.1590/S0104-66322005000100012
15. J. Osuntokun and P. A. Ajibade, J. Nanomater. **2016**, 3296071 (2016). https://doi.org/10.1155/2016/3296071
16. J. Osuntokun and P. A. Ajibade, Physica B: Cond. Matter. **496**, 106 (2016). https://doi.org/10.1016/j.physb.2016.05.024
17. S. I. Sadovnikov and E. Yu. Gerasimov, Nanoscale Adv. **1**, 1581 (2019). https://doi.org/10.1039/c8na00347e
18. S. I. Sadovnikov, Russ. J. Inorg. Chem. **64**, 1309 (2019). https://doi.org/10.1134/S0036023619100115
19. X'Pert HighScore Plus. Version 2.2e (2.2.5), PANalytical B. V. Almedo, the Netherlands, 2009.
20. Match! Version 1.10b, Phase Identification from Powder Diffraction, 2003–2010 Crystal Impact.
21. J. T. S. Van Aswegen and H. Verleger, Die Naturwissenschafien **47**, 131 (1960). https://doi.org/10.1007/BF00628510
22. JCPDS card No. 005-0566.
23. Y. N. Xu and W. Y. Ching, Phys. Rev. B **48**, 4335 (1993). https://doi.org/10.1103/PhysRevB.48.4335
24. D. W. G. Ballentyne and B. Roy, Physica A **27**, 337 (1961). https://doi.org/10.1016/0031-8914(61)90106-9
25. S. I. Sadovnikov, N. S. Kozhevnikova, and A. A. Rempel, Inorg. Mater. **47**, 837 (2011). https://doi.org/10.1134/S0020168511080176
26. S. I. Sadovnikov, N. S. Kozhevnikova, and A. A. Rempel, Russ. J. Inorg. Chem. **56**, 1864 (2011). https://doi.org/10.1134/S0036023611120448
27. S. Kim, R. Merkle, and J. Maier, Solid State Ionics **161**, 113 (2003). https://doi.org/10.1016/S0167-2738(03)00262-5
28. U. Szałaj, Ś. A. Świderska, A. Chodara, et al., Nanomaterials **9**, 1005 (2019). https://doi.org/10.3390/nano9071005
29. M. Drygas, J. F. Janik, and L. Czepirski, Curr. Nanosci. **9**, 318 (2013). https://doi.org/10.2174/1573413711309030004
30. S. I. Sadovnikov and A. I. Gusev, J. Alloys Compd. **586**, 105 (2014). https://doi.org/10.1016/j.jallcom.2013.10.008
31. M. Bhattacharjee and D. Bandyopadhyay, Sens. Actuators, A.: Phys. **285**, 241 (2019). https://doi.org/10.1016/j.sna.2018.11.034
32. S. I. Sadovnikov and A. I. Gusev, J. Therm. Anal. Calorim. **131**, 1155 (2018). https://doi.org/10.1007/s10973-017-6691-8
33. A. K. Orlov, Zapiski Gorn. Inst. **169**, 163 (2006).

Translated by O. Fedorova